

Measurement of Branching Fraction and Search for CP Violation in $B \rightarrow \phi\phi K$

S. Mohanty,^{72,80} A. B. Kaliyar,⁷² V. Gaur,⁸¹ G. B. Mohanty,⁷² I. Adachi,^{15,11} K. Adamczyk,⁵⁴ H. Aihara,⁷⁷ S. Al Said,^{71,34} D. M. Asner,³ H. Atmacan,⁷ V. Aulchenko,^{4,56} T. Aushev,¹⁷ T. Aziz,⁷² V. Babu,⁸ S. Bahinipati,²¹ P. Behera,²³ M. Bessner,¹⁴ V. Bhardwaj,²⁰ T. Bilka,⁵ J. Biswal,³¹ A. Bobrov,^{4,56} A. Bozek,⁵⁴ M. Bračko,^{44,31} T. E. Browder,¹⁴ M. Campajola,^{28,49} D. Červenkov,⁵ V. Chekelian,⁴⁵ A. Chen,⁵¹ B. G. Cheon,¹³ K. Chilikin,⁴⁰ K. Cho,³⁶ S.-J. Cho,⁸⁴ S.-K. Choi,¹² Y. Choi,⁶⁹ S. Choudhury,²² D. Cinabro,⁸² S. Cunliffe,⁸ S. Das,⁴³ N. Dash,²³ G. De Nardo,^{28,49} R. Dhamija,²² F. Di Capua,^{28,49} Z. Doležal,⁵ T. V. Dong,¹⁰ S. Eidelman,^{4,56,40} T. Ferber,⁸ B. G. Fulsom,⁵⁸ N. Gabyshev,^{4,56} A. Garmash,^{4,56} A. Giri,²² P. Goldenzweig,³² B. Golob,^{41,31} O. Grzymkowska,⁵⁴ Y. Guan,⁷ K. Gudkova,^{4,56} C. Hadjivasiliou,⁵⁸ S. Halder,⁷² K. Hayasaka,⁵⁵ H. Hayashii,⁵⁰ W.-S. Hou,⁵³ C.-L. Hsu,⁷⁰ K. Inami,⁴⁸ A. Ishikawa,^{15,11} R. Itoh,^{15,11} M. Iwasaki,⁵⁷ W. W. Jacobs,²⁴ H. B. Jeon,³⁸ S. Jia,¹⁰ Y. Jin,⁷⁷ K. K. Joo,⁶ K. H. Kang,³⁸ G. Karyan,⁸ B. H. Kim,⁶⁵ C. H. Kim,¹³ D. Y. Kim,⁶⁸ S. H. Kim,⁶⁵ Y.-K. Kim,⁸⁴ K. Kinoshita,⁷ P. Kodyš,⁵ T. Konno,³⁵ S. Korpar,^{44,31} D. Kotchetkov,¹⁴ P. Križan,^{41,31} P. Krokovny,^{4,56} R. Kulasiri,³³ M. Kumar,⁴³ R. Kumar,⁶¹ K. Kumara,⁸² Y.-J. Kwon,⁸⁴ K. Lalwani,⁴³ S. C. Lee,³⁸ J. Li,³⁸ L. K. Li,⁷ Y. B. Li,⁵⁹ L. Li Gioi,⁴⁵ J. Libby,²³ Z. Liptak,^{14,*} D. Liventsev,^{82,15} C. MacQueen,⁴⁶ M. Masuda,^{76,62} T. Matsuda,⁴⁷ M. Merola,^{28,49} K. Miyabayashi,⁵⁰ R. Mizuk,^{40,17} T. J. Moon,⁶⁵ R. Mussa,²⁹ M. Nakao,^{15,11} A. Natochii,¹⁴ L. Nayak,²² M. Nayak,⁷³ N. K. Nisar,³ S. Nishida,^{15,11} K. Ogawa,⁵⁵ S. Ogawa,⁷⁴ Y. Onuki,⁷⁷ P. Oskin,⁴⁰ G. Pakhlova,^{17,40} S. Pardi,²⁸ C. W. Park,⁶⁹ H. Park,³⁸ S.-H. Park,⁸⁴ S. Patra,²⁰ T. K. Pedlar,⁴² R. Pestotnik,³¹ L. E. Piilonen,⁸¹ T. Podobnik,^{41,31} V. Popov,¹⁷ E. Prencipe,¹⁸ M. T. Prim,³² M. Röhrken,⁸ A. Rostomyan,⁸ N. Rout,²³ G. Russo,⁴⁹ D. Sahoo,^{72,80} Y. Sakai,^{15,11} S. Sandilya,²² A. Sangal,⁷ T. Sanuki,⁷⁵ V. Savinov,⁶⁰ G. Schnell,^{1,19} J. Schueler,¹⁴ C. Schwanda,²⁶ A. J. Schwartz,⁷ Y. Seino,⁵⁵ K. Senyo,⁸³ M. E. Sevier,⁴⁶ M. Shapkin,²⁷ C. Sharma,⁴³ J.-G. Shiu,⁵³ B. Shwartz,^{4,56} F. Simon,⁴⁵ E. Solovieva,⁴⁰ M. Starič,³¹ Z. S. Stottler,⁸¹ J. F. Strube,⁵⁸ T. Sumiyoshi,⁷⁹ M. Takizawa,^{66,16,63} K. Tanida,³⁰ Y. Tao,⁹ F. Tenchini,⁸ M. Uchida,⁷⁸ Y. Unno,¹³ S. Uno,^{15,11} Y. Usov,^{4,56} S. E. Vahsen,¹⁴ R. Van Tonder,² G. Varner,¹⁴ K. E. Varvell,⁷⁰ A. Vinokurova,^{4,56} V. Vorobyev,^{4,56,40} C. H. Wang,⁵² E. Wang,⁶⁰ M.-Z. Wang,⁵³ P. Wang,²⁵ X. L. Wang,¹⁰ S. Watanuki,³⁹ J. Wiechczynski,⁵⁴ E. Won,³⁷ X. Xu,⁶⁷ B. D. Yabsley,⁷⁰ W. Yan,⁶⁴ H. Ye,⁸ J. H. Yin,³⁷ Z. P. Zhang,⁶⁴ V. Zhilich,^{4,56} and V. Zhukova⁴⁰

(The Belle Collaboration)

¹University of the Basque Country UPV/EHU, 48080 Bilbao

²University of Bonn, 53115 Bonn

³Brookhaven National Laboratory, Upton, New York 11973

⁴Budker Institute of Nuclear Physics SB RAS, Novosibirsk 630090

⁵Faculty of Mathematics and Physics, Charles University, 121 16 Prague

⁶Chonnam National University, Gwangju 61186

⁷University of Cincinnati, Cincinnati, Ohio 45221

⁸Deutsches Elektronen-Synchrotron, 22607 Hamburg

⁹University of Florida, Gainesville, Florida 32611

¹⁰Key Laboratory of Nuclear Physics and Ion-beam Application (MOE) and Institute of Modern Physics, Fudan University, Shanghai 200443

¹¹SOKENDAI (The Graduate University for Advanced Studies), Hayama 240-0193

¹²Gyeongsang National University, Jinju 52828

¹³Department of Physics and Institute of Natural Sciences, Hanyang University, Seoul 04763

¹⁴University of Hawaii, Honolulu, Hawaii 96822

¹⁵High Energy Accelerator Research Organization (KEK), Tsukuba 305-0801

¹⁶J-PARC Branch, KEK Theory Center, High Energy Accelerator Research Organization (KEK), Tsukuba 305-0801

¹⁷Higher School of Economics (HSE), Moscow 101000

¹⁸Forschungszentrum Jülich, 52425 Jülich

¹⁹IKERBASQUE, Basque Foundation for Science, 48013 Bilbao

²⁰Indian Institute of Science Education and Research Mohali, SAS Nagar, 140306

²¹Indian Institute of Technology Bhubaneswar, Satya Nagar 751007

²²Indian Institute of Technology Hyderabad, Telangana 502285

²³Indian Institute of Technology Madras, Chennai 600036

²⁴Indiana University, Bloomington, Indiana 47408

²⁵Institute of High Energy Physics, Chinese Academy of Sciences, Beijing 100049

- ²⁶*Institute of High Energy Physics, Vienna 1050*
- ²⁷*Institute for High Energy Physics, Protvino 142281*
- ²⁸*INFN - Sezione di Napoli, 80126 Napoli*
- ²⁹*INFN - Sezione di Torino, 10125 Torino*
- ³⁰*Advanced Science Research Center, Japan Atomic Energy Agency, Naka 319-1195*
- ³¹*J. Stefan Institute, 1000 Ljubljana*
- ³²*Institut für Experimentelle Teilchenphysik, Karlsruher Institut für Technologie, 76131 Karlsruhe*
- ³³*Kennesaw State University, Kennesaw, Georgia 30144*
- ³⁴*Department of Physics, Faculty of Science, King Abdulaziz University, Jeddah 21589*
- ³⁵*Kitasato University, Sagamihara 252-0373*
- ³⁶*Korea Institute of Science and Technology Information, Daejeon 34141*
- ³⁷*Korea University, Seoul 02841*
- ³⁸*Kyungpook National University, Daegu 41566*
- ³⁹*Université Paris-Saclay, CNRS/IN2P3, IJCLab, 91405 Orsay*
- ⁴⁰*P.N. Lebedev Physical Institute of the Russian Academy of Sciences, Moscow 119991*
- ⁴¹*Faculty of Mathematics and Physics, University of Ljubljana, 1000 Ljubljana*
- ⁴²*Luther College, Decorah, Iowa 52101*
- ⁴³*Malaviya National Institute of Technology Jaipur, Jaipur 302017*
- ⁴⁴*University of Maribor, 2000 Maribor*
- ⁴⁵*Max-Planck-Institut für Physik, 80805 München*
- ⁴⁶*School of Physics, University of Melbourne, Victoria 3010*
- ⁴⁷*University of Miyazaki, Miyazaki 889-2192*
- ⁴⁸*Graduate School of Science, Nagoya University, Nagoya 464-8602*
- ⁴⁹*Università di Napoli Federico II, 80126 Napoli*
- ⁵⁰*Nara Women's University, Nara 630-8506*
- ⁵¹*National Central University, Chung-li 32054*
- ⁵²*National United University, Miao Li 36003*
- ⁵³*Department of Physics, National Taiwan University, Taipei 10617*
- ⁵⁴*H. Niewodniczanski Institute of Nuclear Physics, Krakow 31-342*
- ⁵⁵*Niigata University, Niigata 950-2181*
- ⁵⁶*Novosibirsk State University, Novosibirsk 630090*
- ⁵⁷*Osaka City University, Osaka 558-8585*
- ⁵⁸*Pacific Northwest National Laboratory, Richland, Washington 99352*
- ⁵⁹*Peking University, Beijing 100871*
- ⁶⁰*University of Pittsburgh, Pittsburgh, Pennsylvania 15260*
- ⁶¹*Punjab Agricultural University, Ludhiana 141004*
- ⁶²*Research Center for Nuclear Physics, Osaka University, Osaka 567-0047*
- ⁶³*Meson Science Laboratory, Cluster for Pioneering Research, RIKEN, Saitama 351-0198*
- ⁶⁴*Department of Modern Physics and State Key Laboratory of Particle Detection and Electronics, University of Science and Technology of China, Hefei 230026*
- ⁶⁵*Seoul National University, Seoul 08826*
- ⁶⁶*Showa Pharmaceutical University, Tokyo 194-8543*
- ⁶⁷*Soochow University, Suzhou 215006*
- ⁶⁸*Soongsil University, Seoul 06978*
- ⁶⁹*Sungkyunkwan University, Suwon 16419*
- ⁷⁰*School of Physics, University of Sydney, New South Wales 2006*
- ⁷¹*Department of Physics, Faculty of Science, University of Tabuk, Tabuk 71451*
- ⁷²*Tata Institute of Fundamental Research, Mumbai 400005*
- ⁷³*School of Physics and Astronomy, Tel Aviv University, Tel Aviv 69978*
- ⁷⁴*Toho University, Funabashi 274-8510*
- ⁷⁵*Department of Physics, Tohoku University, Sendai 980-8578*
- ⁷⁶*Earthquake Research Institute, University of Tokyo, Tokyo 113-0032*
- ⁷⁷*Department of Physics, University of Tokyo, Tokyo 113-0033*
- ⁷⁸*Tokyo Institute of Technology, Tokyo 152-8550*
- ⁷⁹*Tokyo Metropolitan University, Tokyo 192-0397*
- ⁸⁰*Utkal University, Bhubaneswar 751004*
- ⁸¹*Virginia Polytechnic Institute and State University, Blacksburg, Virginia 24061*
- ⁸²*Wayne State University, Detroit, Michigan 48202*
- ⁸³*Yamagata University, Yamagata 990-8560*
- ⁸⁴*Yonsei University, Seoul 03722*

We report the measurement of branching fractions and CP -violation asymmetries in $B \rightarrow \phi\phi K$ decays based on a 711 fb^{-1} data sample containing $772 \times 10^6 B\bar{B}$ events. The data were recorded at the $\Upsilon(4S)$ resonance with the Belle detector at the KEKB asymmetric-energy e^+e^- collider. For

for each pion track; and the presence or absence of SVD hits for each pion track. We require that the invariant mass lie between $491 \text{ MeV}/c^2$ and $504 \text{ MeV}/c^2$, which corresponds to a $\pm 3\sigma$ window in resolution around the nominal K_s^0 mass [12].

B -meson candidates are identified with two kinematic variables: the beam-energy-constrained mass $M_{bc} \equiv \sqrt{E_b^2/c^4 - |\sum_i \vec{p}_i/c|^2}$, and the energy difference $\Delta E \equiv \sum_i E_i - E_b$, where E_b is the beam energy, and \vec{p}_i and E_i are the momentum and energy, respectively, of the i -th decay product of the B candidate. All these quantities are evaluated in the e^+e^- center-of-mass (CM) frame. We perform a fit for each B candidate, constraining its decay products to originate from a common vertex. Candidate events with $M_{bc} \in [5.230, 5.289] \text{ GeV}/c^2$ and $|\Delta E| < 0.1 \text{ GeV}$ are retained for further study. The M_{bc} requirement corresponds to approximately $(-16\sigma, +3\sigma)$ in resolution around the nominal B mass [12], and the ΔE requirement denotes a $\pm 10\sigma$ window around zero. We apply such loose requirements on M_{bc} and ΔE as these are used in a maximum-likelihood fit to obtain the signal yield (described later). We define a signal region as $M_{bc} \in [5.272, 5.289] \text{ GeV}/c^2$ and $|\Delta E| < 0.05 \text{ GeV}$.

After application of the above selection criteria, the average number of B candidates found per event selected in data are 1.7 and 1.6 for $B^+ \rightarrow \phi\phi K^+$ and $B^0 \rightarrow \phi\phi K^0$, respectively. In the case of multiple B candidates, we choose the candidate with the lowest χ^2 value for the aforementioned B -vertex fit. From Monte Carlo (MC) simulation the best candidate selection method is found to have an efficiency of 68% (65%) to correctly identify the B -meson candidate in $B^+ \rightarrow \phi\phi K^+$ ($B^0 \rightarrow \phi\phi K^0$) decays. In only about 6% of the total signal events, the B candidate is misreconstructed due to swapping of kaons between the two ϕ candidates, or of one daughter track with that from the rest of the event. Such misreconstructed events are treated as a part of the signal.

The dominant background is from the $e^+e^- \rightarrow q\bar{q}$ ($q = u, d, s, c$) continuum process. To suppress this background, observables based on event topology are used. The event shape in the CM frame is expected to be spherical for $B\bar{B}$ events and jet-like for continuum events. We use an NN [13] to combine the following six variables: a Fisher discriminant formed out of 16 modified Fox-Wolfram moments [14]; the cosine of the angle between the B momentum and the z axis; the cosine of the angle between the B thrust axis [15] and the z axis; the cosine of the angle between the thrust axis of the B candidate and that of the rest of the event; the ratio of the second- to the zeroth-order Fox-Wolfram moments (all quantities are calculated in the CM frame); and the vertex separation along the z axis between the B candidate and the remaining tracks. The NN training and validation are performed with signal and $q\bar{q}$ MC simulated events. The signal sample is generated with the EVTGEN

program [16], assuming a uniform distribution over the three-body phase space of the final state.

The neural network output (O_{NN}) ranges between -1.0 and 1.0 , where events near -1.0 (1.0) are more continuum- (signal-) like. We apply a loose criterion $O_{\text{NN}} > -0.5$ to reduce the continuum background. The relative signal efficiency loss due to this requirement is about 6% (3%) for $B^+ \rightarrow \phi\phi K^+$ ($B^0 \rightarrow \phi\phi K^0$) decays, whereas the fraction of continuum events rejected is 76% (66%). As the remainder of the O_{NN} distribution strongly peaks near 1.0 for signal, it is difficult to model with an analytic function. However, the transformed variable

$$O'_{\text{NN}} = \log \left[\frac{O_{\text{NN}} - O_{\text{NN},\text{min}}}{O_{\text{NN},\text{max}} - O_{\text{NN}}} \right], \quad (1)$$

where $O_{\text{NN},\text{min}} = -0.5$ and $O_{\text{NN},\text{max}} \simeq 1.0$, has a Gaussian-like distribution that is easier to model. Thus, we use this transformed variable in our signal fit.

Backgrounds due to B decays, mediated by the dominant $b \rightarrow c$ transition, are studied with MC samples of such decays. For both $B^+ \rightarrow \phi\phi K^+$ and $B^0 \rightarrow \phi\phi K^0$ channels, the M_{bc} and ΔE distributions are found to peak in the signal region. To investigate the source of these contributions, we inspect the $m_{\phi\phi}$ distribution, which displays several peaks corresponding to the η_c and other charmonium resonances. To suppress these peaking backgrounds, we exclude candidates for which the $m_{\phi\phi}$ value is greater than $2.85 \text{ GeV}/c^2$. This requirement also allows us to compare our results with the earlier ones from Belle [5] and BaBar [9]. We calculate the detection efficiencies for candidate events below the η_c threshold to be 12.4% and 12.0% for $B^+ \rightarrow \phi\phi K^+$ and $B^0 \rightarrow \phi\phi K^0$, respectively.

Charmless backgrounds that do not produce only kaons in the final state may still contribute to the M_{bc} - ΔE signal region when a final-state particle is misidentified. These are studied with a $B\bar{B}$ MC sample in which one of the B mesons decays via $b \rightarrow u, d, s$ transitions with known or estimated branching fractions [12]. Only 40 events survive from an MC sample equivalent to 50 times the size of the data sample. This small component is combined with the events surviving from $b \rightarrow c$ transitions to form an overall $B\bar{B}$ background component. In addition to this $B\bar{B}$ background that does not peak in M_{bc} or ΔE , we can have contributions from $B \rightarrow \phi K K K$ and $B \rightarrow K K K K K$ decays (described later), which have the same final-state particles as the signal.

The signal yield is obtained with an unbinned extended maximum-likelihood fit to the three variables M_{bc} , ΔE , and O'_{NN} . We define a probability density function (PDF) for each event category, i.e., signal, $q\bar{q}$, and $B\bar{B}$ backgrounds:

$$\mathcal{P}_j^i \equiv \frac{1}{2}(1 - q_i \mathcal{A}_{CP,j}) \mathcal{P}_j(M_{bc}^i) \mathcal{P}_j(\Delta E^i) \mathcal{P}_j(O_{\text{NN}}^i), \quad (2)$$

where i denotes the event index, q_i is the charge of the B candidate ($q_i = \pm 1$ for B^\pm), and \mathcal{P}_j and $\mathcal{A}_{CP,j}$ are

the PDF and CP asymmetry, respectively, for the event category j . The latter is defined as

$$\mathcal{A}_{CP} = \frac{N_{B^-} - N_{B^+}}{N_{B^-} + N_{B^+}}, \quad (3)$$

where N_{B^+} (N_{B^-}) is the number of B^+ (B^-) events. We find equal detection efficiencies for the B^+ ($12.3 \pm 0.1\%$) and B^- ($12.4 \pm 0.1\%$) decays. For neutral B decays, we replace the factor $\frac{1}{2}(1 - q_i \mathcal{A}_{CP,j})$ by 1 in Eq. (2). We also do not perform a CP -violation study in this case, since we would need to tag the recoiling B candidate for that, causing further loss in efficiency on top of the small signal yield. As the correlations among M_{bc} , ΔE , and O'_{NN} are found to be small ($\lesssim 5\%$), the product of three individual PDFs is a good approximation for the total PDF. The extended likelihood function is

$$\mathcal{L} = \frac{e^{-\sum_j n_j}}{N!} \prod_i \left[\sum_j n_j \mathcal{P}_j^i \right], \quad (4)$$

where n_j is the yield of event category j , and N is the total number of candidate events. From the fitted signal yield (n_{sig}), we calculate the branching fraction as

$$\mathcal{B}(B \rightarrow \phi\phi K) = \frac{n_{\text{sig}}}{\varepsilon N_{B\bar{B}} [\mathcal{B}(\phi \rightarrow K^+ K^-)]^2}, \quad (5)$$

where ε and $N_{B\bar{B}}$ are the detection efficiency and the number of $B\bar{B}$ events, respectively. In case of $B^0 \rightarrow \phi\phi K^0$, we multiply the denominator by a factor of $\frac{1}{2}$ to account for $K^0 \rightarrow K_s^0$, as well as by the subdecay branching fraction $\mathcal{B}(K_s^0 \rightarrow \pi^+ \pi^-)$ [12].

As the expected yield of the nonpeaking $B\bar{B}$ background is small, and it is distributed similarly to $q\bar{q}$ in M_{bc} and ΔE , we merge $q\bar{q}$ and $B\bar{B}$ backgrounds into a single component. We find that the difference in the O'_{NN} distribution between the two backgrounds contributes a negligible systematic uncertainty. Table I lists the PDF shapes used to model M_{bc} , ΔE , and O'_{NN} distributions for various event categories of $B \rightarrow \phi\phi K$ candidates. The yield and PDF shape parameters of the combined background are floated in $B^+ \rightarrow \phi\phi K^+$. For the neutral channel, however, the background PDF shapes are fixed to their MC values after correcting for small differences between data and simulation, as obtained from the charged decay. Similarly, for the signal components, we fix the M_{bc} , ΔE , and O'_{NN} shapes to MC values and correct for small data-MC differences according to values obtained from a control sample of $B^+ \rightarrow D_s^+ \bar{D}^0$ decays, where $D_s^+ \rightarrow \phi(\rightarrow K^+ K^-) \pi^+$ and $\bar{D}^0 \rightarrow K^+ \pi^-$.

We apply the above 3D fit to $B^+ \rightarrow \phi\phi K^+$ and $B^0 \rightarrow \phi\phi K^0$ candidate events to determine the signal yield (and \mathcal{A}_{CP} in the first case). Figures 2 and 3 show M_{bc} , ΔE , and O'_{NN} projections of the fits. The fit results are listed in Table II. We find signal yields of $85.0^{+10.2}_{-9.5}$ for $B^+ \rightarrow \phi\phi K^+$ and $26.5^{+5.8}_{-5.1}$ for $B^0 \rightarrow \phi\phi K^0$, and an \mathcal{A}_{CP} value of -0.02 ± 0.11 for the first case. We also

apply the 3D fit to $B^+ \rightarrow \phi\phi K^+$ candidate events with $m_{\phi\phi}$ within the η_c region to calculate the signal yield and \mathcal{A}_{CP} value. The corresponding M_{bc} and ΔE projections are shown in Fig. 4, with the fit results listed in Table II. We obtain a signal yield of $73.2^{+9.0}_{-8.3}$ and an \mathcal{A}_{CP} value of $+0.12 \pm 0.12$ in the η_c region. The signal significance is calculated as $\sqrt{-2 \log(\mathcal{L}_0/\mathcal{L}_{\text{max}})}$, where \mathcal{L}_0 and \mathcal{L}_{max} are the likelihood values with the signal yield fixed to zero and for the nominal fit, respectively. We include systematic uncertainties that impact only the signal yield into the likelihood curve via a Gaussian convolution before calculating the final significance.

TABLE I. List of PDFs used to model the M_{bc} , ΔE , and, O'_{NN} distributions for various event categories for $B \rightarrow \phi\phi K$. The notation G, AG, 2G, ARG, and Poly1 denote Gaussian, asymmetric Gaussian, sum of two Gaussians, ARGUS [17] function, and first-order polynomial, respectively.

Event category	M_{bc}	ΔE	O'_{NN}
Signal	G+ARG	2G+Poly1	G+AG
$q\bar{q} + B\bar{B}$	ARG	Poly1	G

To estimate the contribution of $B \rightarrow \phi K K K$ and $B \rightarrow K K K K K$ decays in the M_{KK} signal region (SR), we repeat the 3D fit in the following two sidebands: SB1 is denoted by the sum of ($M_{K_1 K_2} \in [1.04, 1.2] \text{ GeV}/c^2$ and $M_{K_3 K_4} \in [1.0, 1.04] \text{ GeV}/c^2$) and ($M_{K_1 K_2} \in [1.0, 1.04] \text{ GeV}/c^2$ and $M_{K_3 K_4} \in [1.04, 1.2] \text{ GeV}/c^2$), and SB2 is denoted by $M_{K_1 K_2} \in [1.04, 1.2] \text{ GeV}/c^2$ and $M_{K_3 K_4} \in [1.04, 1.2] \text{ GeV}/c^2$. In Fig. 5 we plot the distribution of data events in the $M_{K_1 K_2}$ vs $M_{K_3 K_4}$ plane showing SR, SB1, and SB2. The resonant $B \rightarrow \phi\phi K$ yield in SR is obtained by solving the following three linear equations:

$$N_0 = n_s + r_{a0} \times n_a + r_{b0} \times n_b, \quad (6)$$

$$N_1 = r_{s1} \times n_s + n_a + r_{b1} \times n_b, \quad (7)$$

$$N_2 = r_{s2} \times n_s + r_{a2} \times n_a + n_b, \quad (8)$$

where N_0 , N_1 , and N_2 are the yields obtained in SR, SB1, and SB2, respectively; n_s , n_a , and n_b are the $B \rightarrow \phi\phi K$ yield in SR, $B \rightarrow \phi K K K$ yield in SB1, and $B \rightarrow K K K K K$ yield in SB2, respectively. Lastly, r_{s1} and r_{s2} are the ratios of $B \rightarrow \phi\phi K$ yields in SB1 and SB2 to that in SR; r_{a0} and r_{a2} are the ratios of $B \rightarrow \phi K K K$ yields in SR and SB2 to that in SB1; and r_{b0} and r_{b1} are the ratios of $B \rightarrow K K K K K$ yields in SR and SB1 to that in SB2. All these ratios are obtained from an MC study. We obtain the resonant $B \rightarrow \phi\phi K$ yield in SR (n_s) as $81.8^{+10.1}_{-9.4}$ and $23.7^{+5.7}_{-5.0}$ for the charged and neutral mode, respectively. These n_s values are used in the branching fraction calculation of Eq. (5).

The background-subtracted distributions [18] of $m_{\phi\phi}$ and $m_{\phi K}$ obtained for $B^\pm \rightarrow \phi\phi K^\pm$ below the η_c threshold are shown in Fig. 6. These are broadly compatible with the predictions of a three-body phase space MC

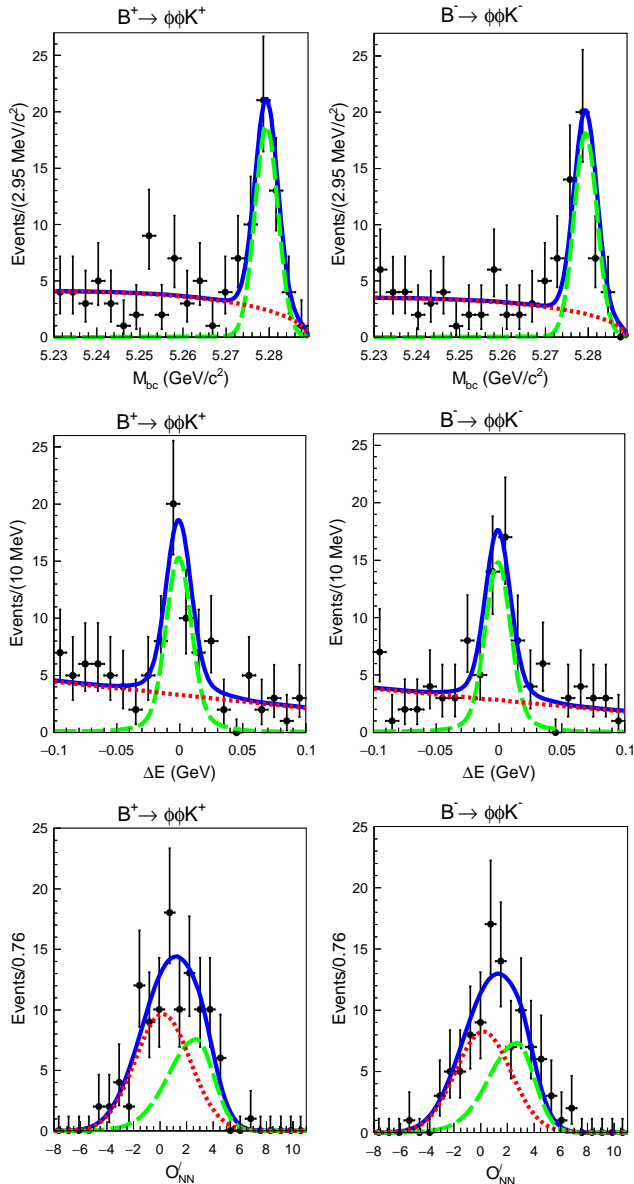


FIG. 2. Projections of $B^\pm \rightarrow \phi\phi K^\pm$ candidate events onto (top) M_{bc} , (middle) ΔE , and (bottom) O'_{NN} . Black points with error bars are the data, solid blue curves are the total PDF, dashed green curves are the signal component, and dotted red curves are the combined $q\bar{q}$ and $B\bar{B}$ background components.

sample. In particular, we do not find any enhancement in the $m_{\phi\phi}$ spectrum, including the $2.3 \text{ GeV}/c^2$ region [3] where a glueball and $X(2350)$ candidates are predicted.

Systematic uncertainties in the branching fraction are listed in Table III. The uncertainties due to PDF shapes are estimated by varying all the fixed shape parameters by their errors. In particular, for fixed signal shape parameters, we vary the data-MC corrections by their uncertainties as determined using the control sample of

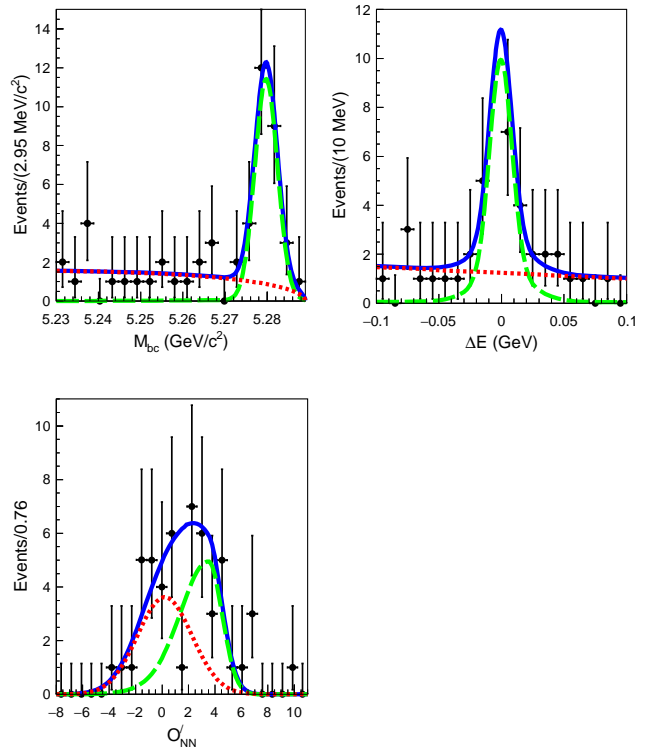


FIG. 3. Projections of $B^0 \rightarrow \phi\phi K^0$ candidate events onto (top left) M_{bc} , (top right) ΔE , and (bottom) O'_{NN} . The legends of the plots are defined in the same manner as in Fig. 2.

TABLE II. Number of candidate events (n_{cand}), detection efficiency (ε), total and resonant signal yield (n_{sig}), significance, branching fraction (\mathcal{B}) and CP asymmetry (\mathcal{A}_{CP}) obtained from a fit to data for $B \rightarrow \phi\phi K$ decays below and within the η_c region. Quoted uncertainties are statistical only, and significances defined in the text are given in terms of standard deviations.

	$B^+ \rightarrow \phi\phi K^+$	$B^0 \rightarrow \phi\phi K^0$	$B^+ \rightarrow \phi\phi(\eta_c)K^+$
n_{cand}	207	51	84
ε (%)	12.4	12.0	15.4
Total n_{sig}	$85.0^{+10.2}_{-9.5}$	$26.5^{+5.8}_{-5.1}$	$73.2^{+9.0}_{-8.3}$
Significance	14.9	7.2	16.7
Resonant n_{sig}	$81.8^{+10.1}_{-9.4}$	$23.7^{+5.7}_{-5.0}$	–
\mathcal{B} (10^{-6})	$3.43^{+0.48}_{-0.46}$	$3.02^{+0.75}_{-0.66}$	–
\mathcal{A}_{CP}	-0.02 ± 0.11	–	$+0.12 \pm 0.12$

$B^+ \rightarrow D_s^+ \bar{D}^0$ decays. Potential fit bias is checked by performing an ensemble test comprising 1000 pseudo-experiments, where signal is taken from the corresponding MC sample, and the PDF shapes are used to generate background events. We obtain a Gaussian normalized residual distribution of unit width, and add its mean and uncertainty in width in quadrature to calculate the systematic error. Uncertainty due to continuum suppression is obtained with the $B^+ \rightarrow D_s^+ \bar{D}^0$

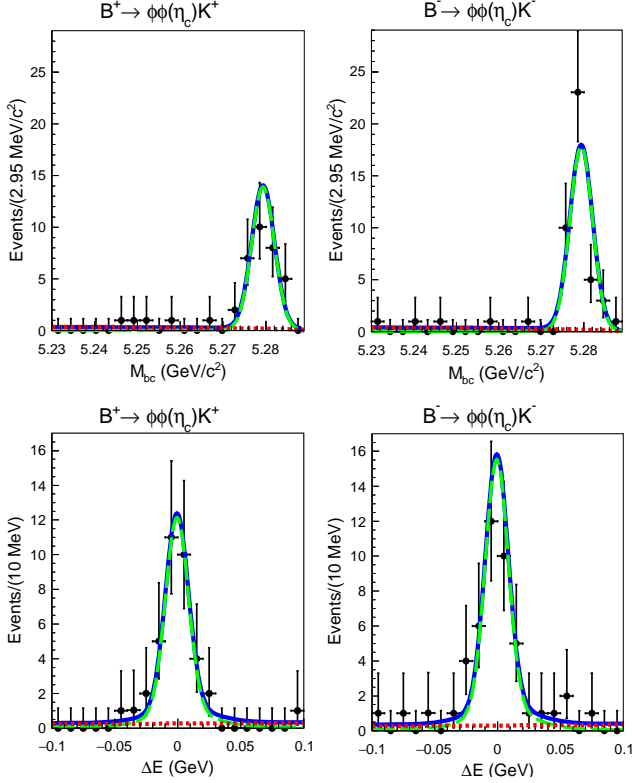


FIG. 4. Projections of $B^\pm \rightarrow \phi\phi K^\pm$ candidate events within the η_c region onto (top) M_{bc} and (bottom) ΔE . The legends of the plots are defined in the same manner as in Fig. 2.

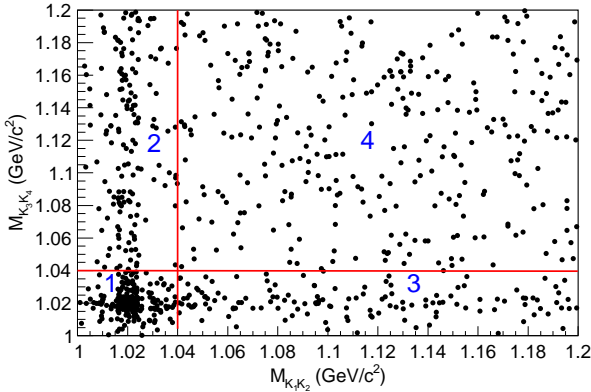


FIG. 5. Distribution of data events in the $M_{K_1K_2}$ vs $M_{K_3K_4}$ plane which shows the M_{KK} signal region (region 1) and two sidebands SB1 (region 2 and 3) and SB2 (region 4).

control sample by comparing, between data and simulation, fit results obtained with and without the O_{NN} requirement. A $D^{*+} \rightarrow D^0(K^-\pi^+)\pi^+$ control sample is used to determine the systematic uncertainty due to the $\mathcal{R}_{K/\pi}$ requirement. We use partially reconstructed $D^{*+} \rightarrow D^0(K_S^0\pi^+\pi^-)\pi^+$ decays to assign the systematic

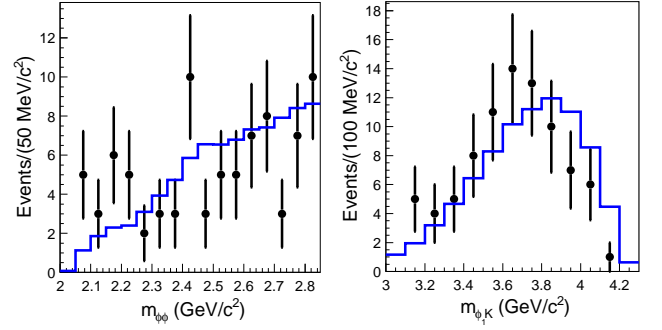


FIG. 6. Background-subtracted signal yield as a function of $m_{\phi\phi}$ (left) and $m_{\phi_1 K}$ (right) for $B^\pm \rightarrow \phi\phi K^\pm$. Black points with error bars are data and solid blue histograms denote the expectation from a phase-space MC sample.

uncertainty due to charged-track reconstruction (0.35% per track). The uncertainty due to K_S^0 reconstruction is estimated from $D^0 \rightarrow K_S^0 K_S^0$ decays [19]. We estimate the uncertainty due to efficiency variation across the Dalitz plot by weighting phase-space-generated signal MC events according to the measured distribution in data (Fig. 6) and taking the difference between the weighted and nominal efficiency. The total systematic uncertainty is obtained by adding all the above contributions in quadrature.

TABLE III. Systematic uncertainties (in %) in the branching fractions. Values listed in the top three rows impact the signal yield and are included in the calculation of signal significance.

Source	$B^\pm \rightarrow \phi\phi K^\pm$	$B^0 \rightarrow \phi\phi K^0$
Signal PDF	+1.5	+1.3
Background PDF	-1.7	-1.9
Fit bias	-	+3.0
Efficiency variation	±1.7	±2.0
$\mathcal{R}_{K/\pi}$ requirement	±2.1	±2.1
$q\bar{q}$ suppression	±5.2	±4.3
Track reconstruction	±0.5	±0.5
K_S^0 reconstruction	±1.8	±1.4
K_S^0 reconstruction	-	±0.9
Number of $B\bar{B}$ events	±1.4	±1.4
Total	±6.5	+6.5 -6.3

We consider two possible sources of systematic uncertainties contributing to \mathcal{A}_{CP} , as listed in Table IV. The first is due to the intrinsic detector bias on charged kaon detection and is estimated using $D_s^+ \rightarrow \phi\pi^+$ and $D^0 \rightarrow K^-\pi^+$ decays [20]. The second arises due to the potential variation of the PDF shapes. We calculate its contribution by following a procedure similar to that used in estimating the PDF shape uncertainties in the branching fractions.

In summary, we have measured the branching fractions and CP -violation asymmetries in $B \rightarrow \phi\phi K$ decays based on the full $\Upsilon(4S)$ data sample of $772 \times 10^6 B\bar{B}$ events

TABLE IV. Systematic uncertainties in \mathcal{A}_{CP} .

Source	$B^\pm \rightarrow \phi\phi K^\pm$	$B^\pm \rightarrow \phi\phi(\eta_c)K^\pm$
Detection asymmetry	± 0.008	± 0.008
Signal PDF shape	$^{+0.002}_{-0.003}$	± 0.002
Total	± 0.01	± 0.01

collected by the Belle detector at the KEKB asymmetric-energy e^+e^- collider. We obtain the branching fraction and CP asymmetry for $B^\pm \rightarrow \phi\phi K^\pm$ below the η_c threshold ($m_{\phi\phi} < 2.85 \text{ GeV}/c^2$) as

$$(3.43^{+0.48}_{-0.46} \pm 0.22) \times 10^{-6} \quad (9)$$

and

$$-0.02 \pm 0.11 \pm 0.01, \quad (10)$$

respectively. We also report the CP -violation asymmetry for $B^\pm \rightarrow \phi\phi K^\pm$ in the η_c region ($m_{\phi\phi} \in [2.94, 3.02] \text{ GeV}/c^2$) to be

$$+0.12 \pm 0.12 \pm 0.01, \quad (11)$$

consistent with no CP violation. The obtained value of the branching fraction of $B^\pm \rightarrow \phi\phi K^\pm$ decay is consistent with and supersedes our previous result [5]. The measured branching fraction for $B^0 \rightarrow \phi\phi K^0$ below the η_c threshold is

$$(3.02^{+0.75}_{-0.66} \pm 0.20) \times 10^{-6}. \quad (12)$$

We find no evidence for glueball production in these decays.

SM acknowledges fruitful discussions with S. Mahapatra (Utkal University). We thank the KEKB group for excellent operation of the accelerator; the KEK cryogenics group for efficient solenoid operations; and the KEK computer group, the NII, and PNNL/EMSL for valuable computing and SINET5 network support. We acknowledge support from MEXT, JSPS and Nagoya's TL-PRC (Japan); ARC (Australia); FWF (Austria); SNSF and CCEPP (China); MSMT (Czechia); CZF, DFG, EXC153, and VS (Germany); DAE, Project Identification No. RTI 4002, and DST (India); INFN (Italy); MOE, MSIP, NRF, RSRI, FLRFAS project, GSDC of KISTI and KREONET/GLORIAD (Korea); MNiSW and NCN (Poland); MSHE, Agreement 14.W03.31.0026

(Russia); University of Tabuk (Saudi Arabia); ARRS (Slovenia); IKERBASQUE (Spain); SNSF (Switzerland); MOE and MOST (Taiwan); and DOE and NSF (USA).

* now at Hiroshima University

- [1] N. Cabibbo, Phys. Rev. Lett. **10**, 531 (1963); M. Kobayashi and T. Maskawa, Prog. Theor. Phys. **49**, 652 (1973).
- [2] M. Hazumi, Phys. Lett. B **583**, 285 (2004).
- [3] C. K. Chua, W.-S. Hou, and S.-Y. Tsai, Phys. Lett. B **544**, 139 (2002).
- [4] Z. Q. Liu *et al.* (Belle Collaboration), Phys. Rev. Lett. **108**, 232001 (2012).
- [5] H. C. Huang *et al.* (Belle Collaboration), Phys. Rev. Lett. **91**, 241802 (2003).
- [6] Inclusion of charge-conjugate reactions is implied unless stated otherwise.
- [7] S. Fajfer, T. N. Pham, and A. Prapotnik, Phys. Rev. D **69**, 114020 (2004).
- [8] C.-H. Chen and H.-N. Li, Phys. Rev. D **70**, 054006 (2004).
- [9] J. P. Lees *et al.* (BaBar Collaboration), Phys. Rev. D **84**, 012001 (2011).
- [10] A. Abashian *et al.* (Belle Collaboration), Nucl. Instrum. Methods Phys. Res., Sect. A **479**, 117 (2002); also see the detector section in J. Brodzicka *et al.*, Prog. Theor. Exp. Phys. **2012**, 04D001 (2012).
- [11] S. Kurokawa and E. Kikutani, Nucl. Instrum. Methods Phys. Res., Sect. A **499**, 1 (2003), and other papers included in this Volume; T. Abe *et al.*, Prog. Theor. Exp. Phys. **2013**, 03A001 (2013) and references therein.
- [12] P. A. Zyla *et al.* (Particle Data Group), Prog. Theor. Exp. Phys. **2020**, 083C01 (2020).
- [13] M. Feindt and U. Kerzel, Nucl. Instrum. Methods Phys. Res., Sect. A **559**, 190 (2006).
- [14] S. H. Lee *et al.* (Belle Collaboration), Phys. Rev. Lett. **91**, 261801 (2003).
- [15] S. Brandt, C. Peyrou, R. Sosnowski, and A. Wroblewski, Phys. Lett. **12**, 57 (1964); E. Farhi, Phys. Rev. Lett. **39**, 1587 (1977).
- [16] D. J. Lange, Nucl. Instrum. Methods Phys. Res., Sect. A **462**, 152 (2001).
- [17] H. Albrecht *et al.* (ARGUS Collaboration), Phys. Lett. B **241**, 278 (1990).
- [18] M. Pivk and F. R. Le Diberder, Nucl. Instrum. Methods Phys. Res., Sect. A **555**, 356 (2005).
- [19] N. Dash *et al.* (Belle Collaboration), Phys. Rev. Lett. **119**, 171801 (2017).
- [20] M. Staric *et al.* (Belle Collaboration), Phys. Rev. Lett. **108**, 071801 (2012).